



Article

High-Resolution Humidity Observations Based on Commercial Microwave Links (CML) Data—Case of Tel Aviv Metropolitan Area

Yoav Rubin ^{*}, Shira Sohn and Pinhas Alpert

Porter School for the Environment and Earth Sciences, Tel Aviv University, Tel Aviv 6997801, Israel

^{*} Correspondence: rubin.yoav@gmail.com

Abstract: The humidity in the atmosphere plays a crucial role in a wide range of atmospheric processes determined by the water-vapor concentration in the air. The accuracy of weather forecasts is largely dictated by the humidity field measured at low atmospheric levels. At the near-surface level, the absolute humidity variations can be large due to the variability of land cover (LC). Cities are one of the primary LCs which have a substantial impact on the humidity field. Large urban areas are expanding, causing a significant change in the near-surface humidity field. Current measurement tools, however, do not satisfactorily assess the cities' effects on the humidity field. This paper presents an innovative method for high-resolution humidity measurements based on the cellular network. Here, the humidity field around Tel Aviv was retrieved from the cellular network during the summer of 2017. The results show a well-noticed impact of the city and other LC types on the humidity field over the Tel Aviv metropolitan area. The method presented here can offer an improved description of the humidity field at the city-canopy level and therefore provide a better assessment of the urban/LC effects on the environment, atmospheric modeling, and particularly on clouds/rain development.

Keywords: urban climate; urban wet island; urban dry island; land use; land cover; semi-arid climate; temperate climate



Citation: Rubin, Y.; Sohn, S.; Alpert, P. High-Resolution Humidity Observations Based on Commercial Microwave Links (CML) Data—Case of Tel Aviv Metropolitan Area. *Remote Sens.* **2023**, *15*, 345. <https://doi.org/10.3390/rs15020345>

Academic Editors:
Giampaolo Ferraioli, Gerardo Di Martino, Alessio Di Simone, Pasquale Imperatore and Hugo Carreno-Luengo

Received: 24 October 2022
Revised: 30 December 2022
Accepted: 3 January 2023
Published: 6 January 2023



Copyright: © 2023 by the authors. Licensee MDPI, Basel, Switzerland. This article is an open access article distributed under the terms and conditions of the Creative Commons Attribution (CC BY) license (<https://creativecommons.org/licenses/by/4.0/>).

1. Introduction

According to the World Urbanization Prospects by the UN [1], 55.3% of the world's population lives in cities. By 2050 this will increase to 68.4%, which the population mainly residing in mega cities spread over vast areas. Those areas are experiencing a fast development, leading to significant land use and land-cover (LC in brief) changes over a large region, resulting in changes in meteorological variables such as temperature and moisture, which are often influenced by the surface characteristics. The differences between rural and urban areas in terms of meteorological variables, especially temperature, are called urban heat islands (UHIs). The rural–urban differences in the humidity levels are called the urban dry or wet island effects [2]. One important meteorological value influenced by the LC over cities is the absolute humidity, or the amount of air water vapor [g/m^3]. Most of the sources for water vapor over continental regions are at the surface; thus, the absolute humidity values are very sensitive to the LC. Since the humidity plays a significant role in many atmospheric processes, measuring it in a high spatial resolution near the surface is essential.

The humidity–spatial rural-to-urban differences have been examined in the past for several cities [3,4], demonstrating the significant role of the LC in determining the humidity values [5,6]. Urban–rural differences are explained mostly by differences in near-surface atmospheric water content, which are attributed to the canopy over urban cores. The urban area can be either a humidity sink or source when compared to the surrounding rural areas; in some cases, the effect of the urban area is positive, and in others it is negative [2]. In addition to other characteristics of the city that have an impact on meteorology such as roughness, aerosols, and albedo, LC is likely to affect the city's

clouds [7]. Some studies have even linked moisture and temperature spatial variability and the nature of precipitation [8–12]. For instance, strong temperature differences ($>1.25\text{ }^{\circ}\text{C}$), enhanced thunderstorm formation, and weak temperature differences ($<1.25\text{ }^{\circ}\text{C}$) produced a minimum, regional, normalized rainfall in the most urbanized area of Beijing [8]. The most important factor for induced precipitation appears to be low-level moisture, rather than UHI intensity [12].

Measuring the humidity around cities is most challenging. Urban areas are characterized by a large LC variability and have a significant impact on many meteorological variables, resulting in a potential impact on weather and, in the long term, on climate. Some typical city LC might influence the air water vapor as, for instance, concrete and roads can prevent surface-water accumulation. On the other hand, cities have many water sources that have a positive effect on the urban-air humidity. For example, human metabolism, vehicles, and several industries, which are deployed in high densities in urban areas, add water vapor to the air [13].

The most common method for measuring the surface humidity today is by using instruments installed $\sim 2\text{ m}$ above the surface at weather stations. At this altitude, the instruments can be easily influenced by their surroundings and show a value which may not be representative for the larger area, i.e., the effect due to the integration of all the city's water sources and sinks. Daramola and Balogun [14] suggested using satellite images in order to estimate the influences of different LCs on the energy balance inside the city of Akure, Nigeria, especially by estimating the LC effect on the air humidity. This approach might be good for examining the influence of different LCs on the environment for specific conditions, but it does not provide in situ humidity measurements. Therefore, satellite data may not be sufficient for weather prediction based on numerical weather prediction (NWP) models. Also, GPS and satellite images can provide information on the vertically integrated water vapor [15–18]. However, the GPS humidity values used for weather forecasts are often not very useful for near-surface spatial variability monitoring due to different LCs.

In order to evaluate the city effect on the humidity field, it is necessary to measure the integration of all the water sources and sinks around the city. Therefore, it is more efficient to measure the humidity at a higher level above the ground, i.e., the “city canopy.” The evaluation of the humidity at the city canopy is important, not only for the assessment of the city effect, but also to obtain a better description of the near-surface humidity field fed into the NWP models. Increasing the resolution of the humidity measurements is therefore likely to improve the rainfall forecast near the cities and the assessment of the city effect on the rain pattern and characteristics. Classical humidity instruments are rarely positioned at the canopy level. Therefore, there is not enough information on the humidity at the most critical altitude for the development of clouds and rain.

The present novel CML (commercial microwave links) tool for measuring humidity is positioned at an average altitude of $\sim 30\text{ m}$ [19]. Thus, a more reliable description of the humidity field can be received at a specific height above the city, exactly where important atmospheric exchange processes take place, but no classical instruments are available.

The cellular data was shown to improve atmospheric monitoring for several parameters, including rain [20–24], fog [25], moisture [26,27], dew [28], and pollution [29], etc. [30]. Some methods were developed for investigating the observations' errors [31–34] and reconstructing the rainfall fields [35–37]. The technique for retrieving the humidity introduced in this study was originally proposed by [26] and was improved later by [27] in order to map atmospheric surface humidity using CML data. This was the basis for mapping the humidity field over the north of Israel in high resolution, which was proven to be more accurate than ERA-Interim reanalysis by the ECMWF (European Centre for Medium-Range Weather Forecasts) [19].

In the present study, humidity measurements at high spatial resolution are used to better understand how cities and different LCs affect weather. A description of the method used to retrieve humidity from CMLs is provided in Section 2, along with extensive information about the study region and CML characteristics. The results of this study are

presented and discussed in Section 3. Section 3 consists of three subsections: Section 3.1 demonstrates the quality of CML observations via a comparison with weather stations, and Sections 3.2 and 3.3 analyze the effects of LCs on near-surface humidity over the study region.

2. Methods

2.1. Research Area and Period

Here, we have focused on the larger Tel Aviv Metropolitan area, including the city of Netanya in the north and Ashdod in the south (Figure 1, 34.6–35.3E, 31.6–32.58N). Most of the study area is a low plain lying between the Mediterranean Sea in the west and the Judea–Samaria mountains to the east. This region is characterized by different LCs such as: urban areas, vegetation, agriculture, highways, airports, and industrial areas, etc. The proximity to the sea has a significant impact on the humidity values, which are often high next to the coastline and decrease eastward. Weather stations located close to the sea usually show high absolute humidity values that may represent a very small area on seashore and thus are not suitable for comparison with the links that are inland. Large differences were observed at stations that are located 5 km or further from the coastline (Figure S1). This might be related to local factors such as land cover.

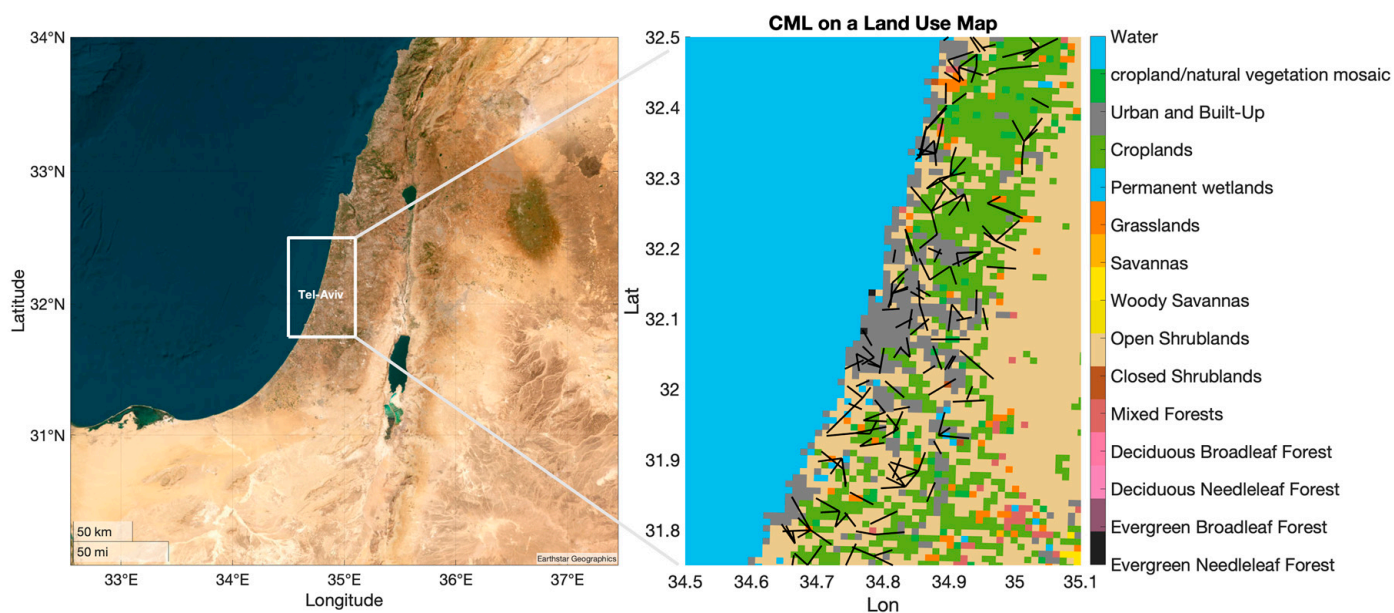


Figure 1. A map of 388 links with lengths between 2–10 km and frequencies of approximately 23 GHz on a land-use map. Land-use types are shown on the color bar to the right (https://www2.mmm.ucar.edu/wrf/users/download/get_sources_wps_geog.html, accessed on 23 October 2022).

We examined a period of one month in the summer, July 2017, during which the measurements were instantaneous at 3 am local time. In general, the conditions in Israel during the summer nights are good for examining the effect of the LC on the humidity field. During this season, the weather patterns are semi-permanent with small inter-daily changes mostly due to the Persian Trough, which is centered to the east around the Fertile Crescent and varies in its intensity (i.e., weak, medium, or strong [38]). These changes affect the height of the inversion layer above Tel Aviv, which is reflected in the humidity changes [39]. The relative humidity and the inversion are, in general, negatively correlated, i.e., the humidity is high with low inversion and vice versa. These changes are noticeable, but do not have an impact on the humidity signature by different LCs. This is due to the land breeze, a weak, nocturnal eastern wind from the land toward the sea. This phenomenon is very common along the shoreline plains during summer [40,41]. The combination of

the unique conditions of a strong, boundary-layer stability at night for the whole summer provides the opportunity to examine the LC effect on the humidity field.

2.2. Links Characteristics

Maps of the average absolute humidity were produced for examining the LC effect on the absolute humidity field. The maps were based on 388 links over the center part of Israel from two cellular companies: PHI and Cellcom (Figure 1). The links' lengths employed here were between 2 and 10 km. Links below 2 km were not able to capture the received signal level (RSL) changes due to the humidity, since those changes are smaller than the measurements' quantization error (the minimum interval between the measurements). Additionally, links above 10 km would not capture the humidity spatial variability well, which may change dramatically around sources/sinks of humidity (see Section 2.3).

In order to isolate the LC's effect, the links' characteristics were similar, as follows. All the links are under a 200 m AMSL (Above Mean Sea Level), with an average AMSL altitude of ~56.5 m, and all links were included in the interpolation, even those showing lower correlations with the weather stations. The number of links between two latitudes with a 0.2 deg interval was similar to the average altitude AMSL of ~55.5 m, and the range of the heights above the surface was from 1 to 87 m, with an average of ~25.5 m.

2.3. CML-Based Humidity Retrievals

The attenuation of a microwave signal due to water molecules is most significant at the resonance line of 22.235 GHz [26]. Based on Equation (1) [42,43], [Rec ITU-R P.676-13, 2022], and assuming no rainfall, fog, clouds, or strong winds, we can estimate the specific attenuation of dry air and water vapor (WV) as follows:

Here, γ_v and γ_d are the specific attenuation due to WV and dry air (i.e., oxygen, pressure-induced nitrogen, and non-resonant Debye attenuation), respectively. \tilde{Noise} refers to all other factors that can affect a signal besides WV. Among microwave signals with frequencies around the resonance line of water molecules, γ_d and \tilde{Noise} are usually one order of magnitude smaller than γ_v , with the exception of strong diurnal patterns and erratic noises. Thus, measuring RSL and relating it to WV is possible by:

$$\gamma = \gamma_v + \gamma_d + \tilde{Noise} \quad (1)$$

$$\gamma_v = 0.182f N''(f), \quad \text{where, } N''(f) = \sum_{i(\text{Oxygen})} S_i F_i + N''_D(f) + \sum_{i(\text{Water Vapour})} S_i F_i \quad (2)$$

$N''(f)$ is the imaginary part (absorption) of the complex refractivity, which is a function of the link's frequency f (GHz), pressure p (hPa), temperature T ($^{\circ}\text{C}$), and WV density ρ (g/m^3), which is the quantity to be retrieved from the measured signal γ . $N''(f)$ can be expressed as a function of S_i , the strength of the i -th WV line, and F_i is the WV line shape factor. $N''_D(f)$ is the dry continuum due to pressure-induced nitrogen absorption and the Debye spectrum. Further information on spectroscopic data for WV attenuation can be found at Rec ITU-R P.676-12 (2022). Inverting Equation (2) allows us to calculate the humidity (in WV density units) by knowing the WV specific attenuation, γ_v . Here, T and p are required along the path of links. When compared with errors caused by the minimal interval of the RSL measurements (i.e., the quantization error, QE) [19,26,44], an approximation of T and p caused smaller errors in humidity calculations. The error range can be explained primarily by the QE and CML length [45]. This error comes from dividing the WV attenuation by the link's length in order to obtain the normalized attenuation in dB/km, resulting in the average value of the true humidity along the link's path.

Longer CMLs provide better signal-to-noise ratios; however, we might miss spatial variations along the path of the link. Alternatively, short CMLs may pose a problem when it comes to measuring the true temporal variations in humidity (if errors are too high, the low signal-to-noise ratio makes it difficult to separate physical variations from noise fluctuations). Therefore, the CMLs in this study are limited to 2–10 km in length.

Following the definition of the best CML characteristics for the humidity observations, we are using weather station data to calibrate each link, i.e., finding the RSL base level for the specific attenuation by the WV (γ_v), as is described in the next section.

2.4. Calibration

The γ_d of each CML at the given air conditions varies because each CML has its own total attenuation range and characteristic (length and frequency).

The total attenuation, γ , is defined by Equation (3):

$$\gamma = \text{TSL} - \text{RSL} \quad (3)$$

The attenuation is defined as the difference between the transmit signal level (TSL) and the received signal level (RSL). Following Equation (3), γ_d may be expressed as in Equation (4), i.e., by defining the RSLo, the dry-air contribution to the total RSL.

$$\gamma_d = \text{TSL} - \text{RSLo} \quad (4)$$

Combining Equations (1), (3) and (4), the RSLo can be expressed as in Equation (5), (since the average was calculated over a period, noise can be ignored).

$$\text{RSLo} = \text{RSL} - \gamma_v \quad (5)$$

As a result, we must determine the RSLo for each link. Our analysis indicates that the RSLo does not vary heavily from day to day, especially within the same time of day and season. Using measurements of WV at stations, we estimated the RSLo for nearby links. For specific conditions described above, the humidity observations at a weather station, WS-HO and nearby CMLs, CML-HO, should have similar median values over a period of time. In order to obtain the RSLo, we used past RSL values of the link (RSLp) and past humidity observations at stations, WS-HOPs. Using the past WS-HOPs as a proxy of CLM-HOPs along the CML, we estimated the past values of γ_v at the link, γ_{vp} , using Equation (2), and retrieved the RSLo from Equation (5) as follows:

$$\text{RSLo} = \text{RSLp} - \gamma_{vp} \quad (6)$$

Equation (6) was calculated over a period of two weeks. For each link, the median RSLo for the two weeks period was used to calculate future γ_v values. Equations (3) and (4) are subtracted to calculate γ_v as follows:

$$\gamma_v = \text{RSL} - \text{RSLom} \quad (7)$$

In earlier works [26,27], in order to estimate the RSLo, the WS-HOP and the γ_{vp} were calculated based on the closest weather stations to the CML. When there was a substantial height difference between two stations, such as over complex terrains, the nearest station to a CML may exhibit different humidity patterns than the CML itself. Consequently, in [19] and [45] and in this study, we used a different method. First, the median of the WS-HO, WS-HOm, from each weather station over the study area was calculated for a two-week period. Last, calibration (finding the RSLo for each CML) was performed, assuming that the absolute humidity decreases with elevation AMSL.

Linear equation relationships between the WS-HOm at each station and its height AMSL, h , over the study area, were derived. These equations represent the absolute humidity dependence on the AMSL height over the study region. The calculations were performed for the period between 18 June and 31 June 2017. Once this linear equation was derived, the mean heights AMSL (h) of each CML could then be used to calculate the values of WS-HOm needed to derive the RSLo:

$$\text{WSHOM}(h) = -0.024h + 17.73 \quad (8)$$

Equation (8) describes the resulting linear dependence of $WSHO_m$ on h , the elevation AMSL.

To produce the fitted Equation (8), we used two weeks of data obtained in the period prior to the study because the linear dependence might change based on season and climate zone. In this study, the CML's maximum elevation was limited to 200 m AMSL, and most of the CMLs were under 100 m AMSL (Figure 2). Thus, the $WSHO_m$ was approximately the same value ($\sim 17 \text{ g/m}^3$). The chosen study area was in a low plane in order to examine the spatial humidity variations independent of elevation.

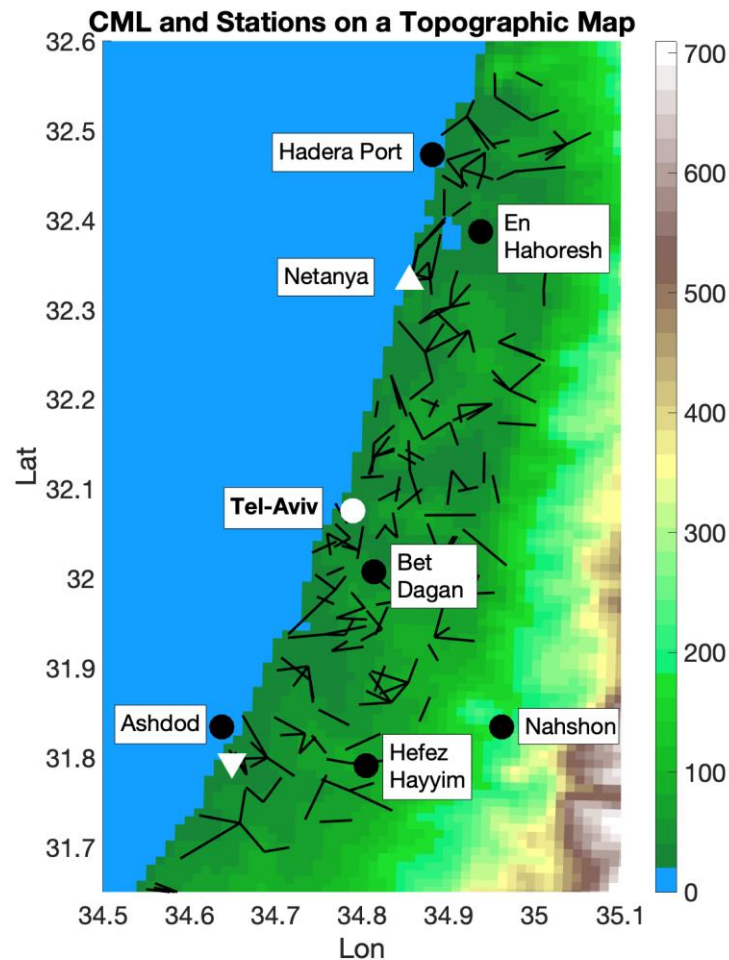


Figure 2. CMLs (black lines) and 7 IMS (Israeli Meteorological Service) weather stations (denoted by the black circles and their names; see Table S1) on a topographic map (https://www2.mmm.ucar.edu/wrf/users/download/get_sources_wps_geog.html, accessed on 23 October 2022). The white circle denotes the coastal city of Tel Aviv; white triangles indicate the coastal cities of Netanya (upward) and Ashdod (downward).

At the time of the measurements (at night), there was a night land-breeze with weak wind blowing from land toward the sea [39]. This created good conditions for examining the spatial humidity patterns. The warm summer night with the weak wind caused the low level of the atmosphere of ~ 10 s meters above the surface to be well-mixed, thus allowing the comparison between the WS-HO and CML-HO at different heights above ground level.

2.5. Interpolation Method

The estimation of the humidity field over a region was performed by interpolation, in which each link was represented by three points with one on each side of the link and one in its middle. In this study, we used the IDW (inverse distance weight) interpolation when the radius of interpolation was 10 km [46]. Choosing a small radius of interpolation emphasizes the spatial changes and the differences between links that represent different regions around the city (see Section 3.2 and Figure S2 for further explanation). Here, the main objective was to determine the effect of local characteristics on the humidity field; therefore, all the links were included in the interpolation and not only those that showed a better correlation with the closest weather stations, as was the case in previous works [19].

3. Results and Discussion

The results of this study were divided into three subsections. The first subsection focuses on the quality of the CMLs observations. A comparison between the CMLs' humidity fields and the weather stations over the study region was made in order to assess the CMLs' performances in a similar manner to pioneering works in the field [19,45]. The second and third subsections focus on the way the LCs over the study region influenced the near-surface humidity. This was examined using two different methods: (1) averaging the CMLs' humidity fields over the region for different synoptic conditions, in order to investigate the effects of the flows and the seasonal inversion on the humidity values, with an emphasis on the LC and spatial characteristics (Section 3.2), and (2) averaging small parts of the region by slicing it into several strips: two strips along the coastline with a north–south orientation; coastal and inner strips (both 9 km wide); and another three west–east oriented strips along the three main cities' latitudes. The width of the strips along the coastline were chosen to be 9 km due to the special characteristics of the coastal lowland's structure in terms of land use. The main cities we focused on are located on a relatively narrow area next to the shore, and most of the croplands are relatively far away from the shore. This is because the weather and climate conditions, as well as the soil characteristics, make the inner strip much more suitable for the development of agriculture and the coastal strip to be more suitable for the development of urban areas around the cities of Netanya and Ashdod.

3.1. Validation and Performances Assessment

For validation, the correlation with seven weather stations from the Israeli Meteorological Service (IMS), as well as the root mean square deviation (RMSD), the mean, and the standard deviation (STD) were calculated. Most of the stations showed good results with the CMLs (Figure 3 and Table S1). Well-noticed were the CMLs' high correlation values. The RMSDs were lower for the CMLs at most of the stations; however, they were lower on average for the ERA5. The mean values showed better results for the CMLs on average, but the STD was better for the ERA5 reanalysis. This can be explained by the synoptic variations that control the summer humidity changes that were well-captured by the reanalysis. When compared to the Spring results obtained by [19], the CML-HO STD is closer to the WS-HO STD due to the dominance of mesoscale weather phenomena, which often control the spring humidity changes and are difficult to be captured by the reanalysis due to its relatively low resolution.

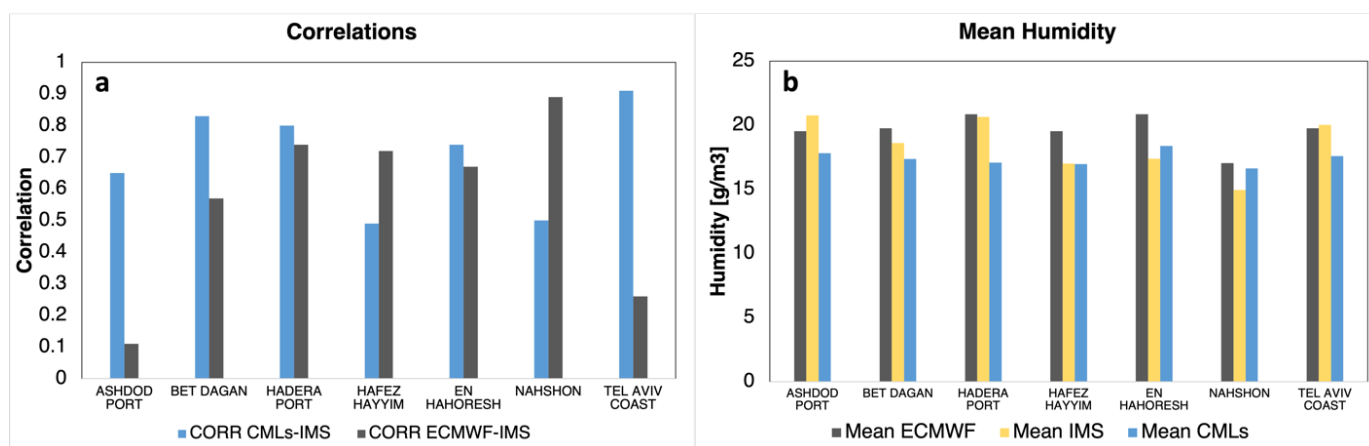


Figure 3. (a): Correlations between the CMLs and the reanalysis from the ECMWF (ERA5) and the Israeli Meteorological Service (IMS). (b): Mean absolute humidity values in $[g/m^3]$ from the CMLs, ECMWF (ERA5), and the IMS. All results refer to observations made during July 2017 of one instantaneous measurement at 3 am. Detailed information and additional results can be found in Table S1.

3.2. Humidity Maps: Average for July 2017

Different radii of interpolation were examined. The maps in Figure S2 show the humidity field averages for the whole period, with an effective radius of 10 km (S2a), effective radius of 20 km (S2b), and effective radius of 30 km (S2c). Finally, we choose 10 km to be the effective radius for this study, in order to examine relatively small-scale spatial patterns caused by LCs. When the effective radius is larger, the general effect of the region around Tel Aviv is positive, i.e., the LC is adding water vapor to the air, in particular to the north part of this region which is characterized by more irrigated fields. When the effective radius is smaller, the signatures of different LCs are noticeable and there are some patches of high humidity values above non-urban areas with high vegetation percentages due to agriculture (Figures 1 and 4). For example, around Netanya, the Sharon area is characterized by intensive agriculture, especially in the northeast part of the region. Additionally, the south part of Tel Aviv and the area around Ashdod are characterized by high humidity. The region east of Ashdod is very similar to the area north of Tel-Aviv, with more irrigated fields. The region between Tel Aviv and Ashdod has lower humidity values on average. A possible explanation for this could be the lack of agriculture and vegetation around this region. This region is dominated by large dunes in the west and an urban area in the east (the cities of Rishon–Letzion and Rehovot). Based on the whole period average, the effects of different LCs on the humidity are prominent. The atmospheric synoptic conditions during the time of the measurements were semi-permanent, but sometimes there were small, inter-daily changes due to the deepening or weakening of the Persian Trough. The variation in the Persian Trough strength mostly affects the inversion height and, consequently, the water vapor concentrations beneath the inversion increase. In this study, the effects of different atmospheric conditions were examined, relying on the synoptic classification by [38]. The main synoptic condition that the study area experienced in July 2017 were Persian Trough–Weak for 16 days, and Persian Trough–Medium for 11 days. Another synoptic system which has influenced the region was High to the West, lasting four days. Figure 4b–d show the average absolute humidity for those three synoptic systems that are controlling the conditions over the study area. The maps show quite similar humidity patterns with high and low values around the aforementioned areas with slight differences. First, the main difference between the two Persian Trough maps is the humidity value, and not the location or the size of the high- and low-value areas. During the medium Persian Trough, the humidity tends to become higher, due to the strengthening of the western winds from the Mediterranean Sea as the Persian Trough deepens. The

opposite occurs during a weak Persian Trough when the western winds weaken. During a High to the West system, the dominant flow is north–west; hence, additional humidity penetrates this region from the sea and causing humidity increases, mostly along the shore around the same spots, but in a different pattern from the other pressure systems. The high-pressure system conditions are rare at this time of the year, and further research is needed for a better understanding of the phenomenon.

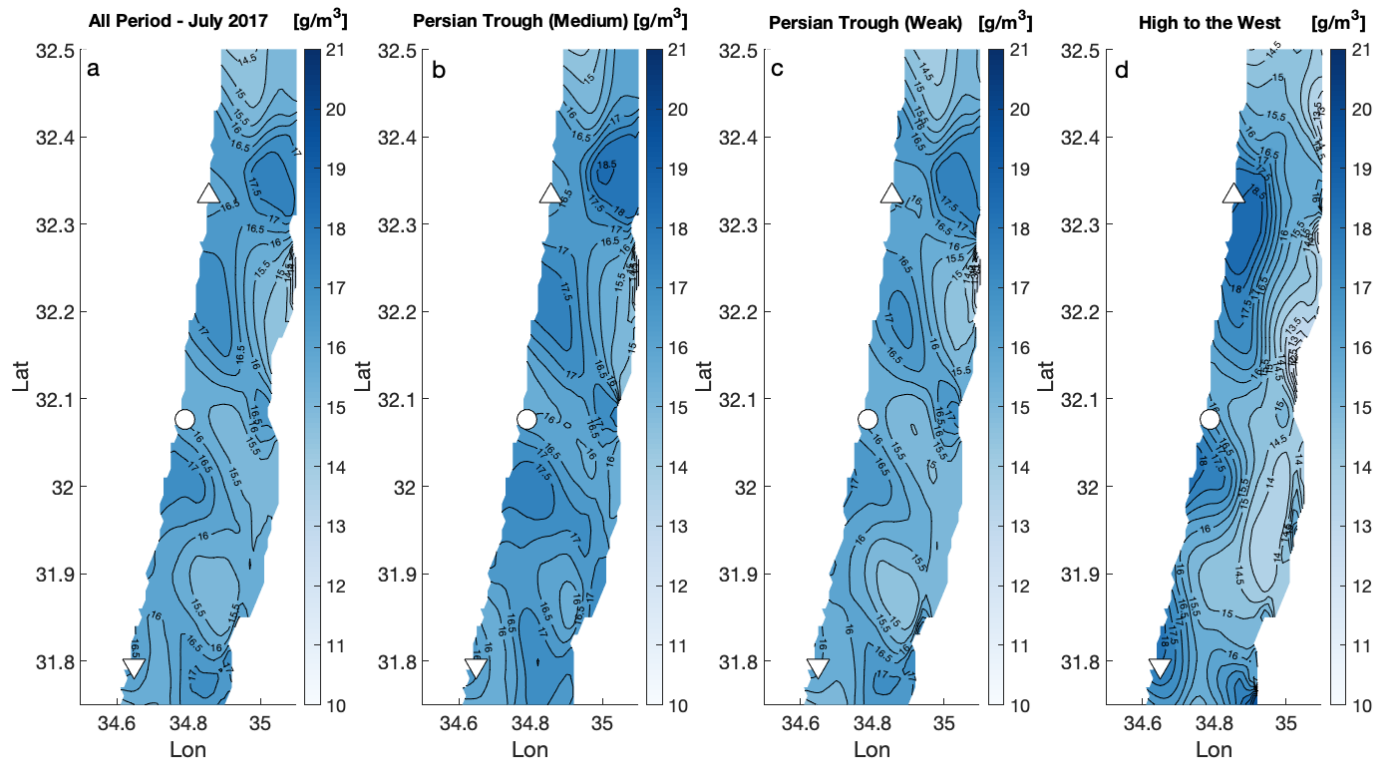


Figure 4. Average humidity maps for the whole period during July 2017 (a) and for three synoptic conditions: medium Persian Trough (b), weak Persian Trough (c), and High to the West (d). Maps (b–d) show the interpolated humidity fields based on 10 km radius of interpolation. White circles denote the coastal cities of Tel Aviv; white triangles are the coastal cities of Netanya (upward) and Ashdod (downward).

3.3. LC and the Humidity Cross-Sections for Different Latitudes

The average maps provide a unique view of the LC effect on the humidity field in the summer conditions. It is apparent that the surface humidity is strongly influenced by the LC, which changes the amount of water released into air. Dry and urban areas seem to reduce the amount of water vapor in the atmosphere when compared to cropland/agriculture, which cover the large area around the city. For a better understanding of the LC's effect on the surface humidity, the cross-sectional averages for different areas (described in Figure 5) were calculated and are shown in Figure 6. Figure 6a shows the cross-section humidity averages for two strips along the coastline, the first 9 km from the shore (coastal strip, Figure 5) and the area between 9 and 18 km from the shore (inner strip, Figure 5). Additionally, the average for the full strip (0–18 km), is presented in Figure 6a.

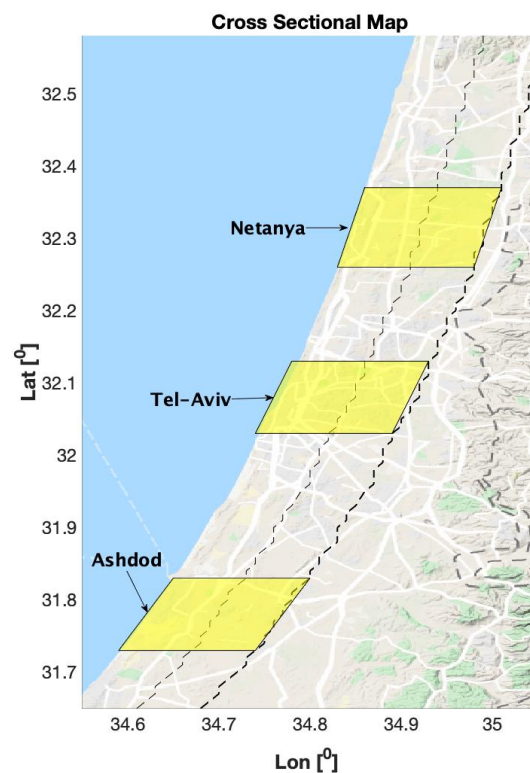


Figure 5. The boundaries of the strips representing the area on which the cross-sectional averages were drawn in Figure 6 are shown. Two NE-SW strips along the coast (dashed line) and three W-E strips around the three cities, Netanya, Tel-Aviv, and Ashdod (yellow parallelograms), are plotted.

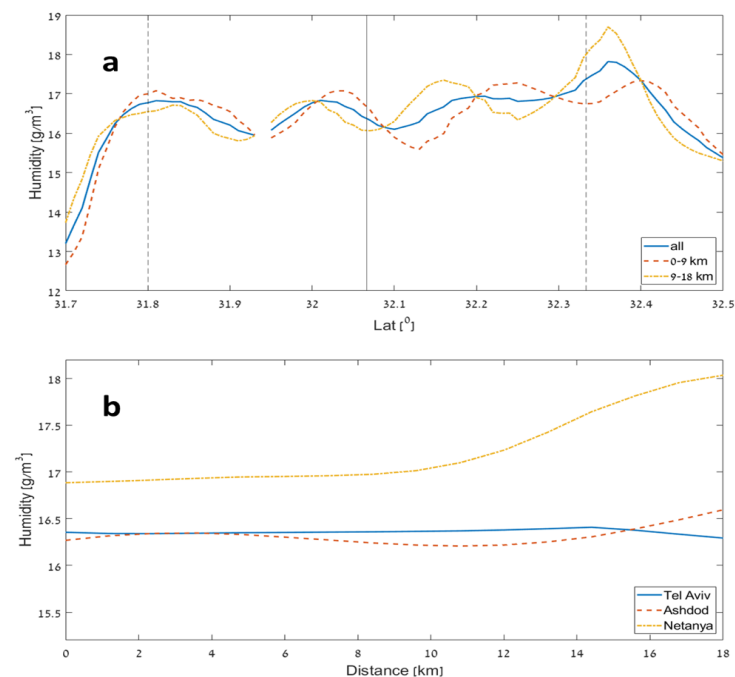


Figure 6. (a) A cross-section of humidity averages for two strips along the coastline: the first 9 km from the shore (red dashed line, coastal strip) and the area between 9 and 18 km from the shore (yellow line, inner strip), and the average humidity for the full 18 km strip (blue solid line). The Tel Aviv latitude is indicated by the solid vertical line, and Ashdod and Netanya latitudes are represented by the dotted vertical lines, with Ashdod in the south and Netanya in the north. (b) A cross-section of humidity averages as a function of the distance from the coast for Netanya (yellow), Tel-Aviv (blue), and Ashdod (red).

In the northern part, the average of the coastal strip shows a near-mirror-image with respect to the inner strip, when around the city of Netanya it is drier than the inner agricultural strip. This behavior is the opposite of what one would expect, which is more humid air at the coastal strip. In contrast, in the southern area, around the city of Ashdod, a more intuitive result is obtained, where the humidity decreases with the distance from the sea. The border between those two regions is the great metropolitan area of Tel Aviv City. Hence, the south part of Tel Aviv City behaves like Ashdod City, while the north part of Tel Aviv fits the humidity structure near Netanya City better. These results highlight the large differences between the climatic characteristics of the two parts of the study region, i.e., the semi-arid Ashdod vs. the temperate, Mediterranean climate zone of Netanya, both just 70 km apart [39].

Around the city of Netanya, which is located in a more temperate climate in the north part of the study region, the city area is found to be drier than the area around it (which is characterized by intensive agriculture, which may have a significant impact during the summer due to irrigation). These findings fit previous studies pointing to the tendency towards reduced humidity over city centers [47,48]. At the southern part around Ashdod City, however, the opposite occurs, and the city area is wetter. Ashdod is primarily influenced by the arid region further south, characterized by a dry climate with lower humidity values. This fact makes the City of Ashdod a humidity source; therefore, the city humidity effect is positive (Figure 6a). A similar phenomenon was shown by [49] for the city of Dubai, which is located in a dry (arid) climate and acts as a humidity source when compared to its surroundings.

In summary, for the wider strip (0–18 km, Figure 6a), Tel Aviv's latitude (32.06 N) has lower mean humidity values than northern and southern latitudes nearby, since Tel Aviv occupies the full zone of the wide strip (blue line, Figure 6a). However, in both Netanya and Ashdod the wider strip shows a peak because of the aforementioned LC reasons. There is a significant humidity increase near Netanya due to the agriculture activity in the east, while the increase near Ashdod occurs due to the city effect in the west.

4. Conclusions

Air humidity is a crucial parameter in many atmospheric processes, mostly in those related to development of clouds and rain. The prediction of rain relies on the humidity measurements, and the resolution of these will determine the weather-forecast accuracy. The humidity at the height of a few tens of meters above surface is highly influenced by the surface characteristics. In many cases, the LC is responsible for the spatial variation of the surface humidity field; therefore, it is a major factor in determining the conditions for rainfall. Measuring the high-resolution surface humidity, where most of the humidity's sinks and sources are, is a challenge with the common tools that are available today. A new approach for measuring the humidity based on the cellular network provides high-resolution information about the surface humidity and, for the first time, allows researchers to examine the LC effect—in particular, the urban effect—on the surface humidity field.

In this study, we examined the humidity field in the region around the large urban area of Tel Aviv City. The atmospheric conditions we chose for this research were during the summer synoptic conditions, characterized by warm nights with a weak night (land) breeze and no rain events. We could therefore obtain a better assessment of urban effect on the humidity field and provide a more accurate picture of the city's urban signature.

The main conclusions of this study are:

- The humidity field is influenced by different LCs, with high humidity observed above agricultural areas that are characterized by vegetation and are often irrigated during the dry summer period.
- Around the urban areas, the absolute humidity values are found to be lower compared to the surrounding area when the city is located in a wetter, temperate Mediterranean climate (e.g., Netanya) and higher when the city is located in a dry, semi-arid climate (e.g., Ashdod).

- The large metropolitan area of Tel Aviv shows a combination of both characteristics due to its location, being just on the semi-arid border.

This research provides a better assessment of the city's effect on humidity and consequently on the weather in general. This is especially important in cases when surface humidity plays a crucial role in the development of clouds and extreme rain events that can lead to severe impacts. The specific scientific and academic contribution of the present research is to highlight the importance of having reliable data on the city's effect on near-surface humidity in order to better understand the real climate of the city and to consequently be able to accurately simulate the city's effects on its climate and future neighborhoods. This is particularly pertinent in the era of urbanization we are living in today.

Supplementary Materials: The following supporting information can be downloaded at: <https://www.mdpi.com/article/10.3390/rs15020345/s1>, Figure S1: The median humidity from several weather stations along the Israeli coastline as a function of the distance from the sea; Figure S2: The average humidity field for the July 2017 (one instantaneous measurement every night at 3 am), for 10 km (a), 20 km (b), and 30 km (c) radius of interpolation; Table S1: Four Skills Comparison for the Three Data Sources for July 2017.

Author Contributions: Y.R.: Conceptualization, Methodology, Software, Formal analysis, Investigation, Data Curation, Writing—Original Draft, Visualization, Project administration. S.S.: Software, Validation, Writing—Review & Editing. P.A.: Conceptualization, Methodology, Resources, Supervision, Writing—Review & Editing, Funding acquisition. All authors have read and agreed to the published version of the manuscript.

Funding: This research was funded by Deutsche Forschungsgemeinschaft grant number 254695484, and the European Union grant number 101037193.

Data Availability Statement: The data are found in the Israeli Atmospheric and Climatic Data Center (IACDC) in Tel Aviv University. Please address the corresponding author for data requests.

Acknowledgments: The authors are grateful to the cellular companies Cellcom and PHI for providing the microwave data, pro bono, for our research. Special thanks to the Israeli Meteorological Service for the meteorological data.

Conflicts of Interest: The authors declare no conflict of interest. The funders had no role in the design of the study; in the collection, analyses, or interpretation of data; in the writing of the manuscript; or in the decision to publish the results.

Abbreviations

AMSL	Above mean sea level
CML	Commercial microwave links
CML-HO	CML humidity observations
ECMWF	European Centre for Medium-Range Weather forecasts
IMS	Israeli Meteorological Service
LC	Land cover
NWP	Numerical weather prediction
QE	Quantization error
RMSD	Root mean square deviation
RSL	Received signal level
STD	Standard deviation
TSL	Transmit signal level
UHI	Urban heat island
WS-HO	Weather station humidity observations
WV	Water vapor

References

1. United Nations. *World Urbanization Prospects: The 2018 Revision*; United Nations: New York, NY, USA, 2019. [\[CrossRef\]](#)
2. Luo, Z.; Liu, J.; Zhang, Y.; Zhou, J.; Yu, Y.; Jia, R. Spatiotemporal characteristics of urban dry/wet islands in China following rapid urbanization. *J. Hydrol.* **2021**, *601*, 126618. [\[CrossRef\]](#)
3. Richards, K. Urban and rural dewfall, surface moisture, and associated canopy-level air temperature and humidity measurements for Vancouver, Canada. *Bound.-Layer Meteorol.* **2005**, *114*, 143–163. [\[CrossRef\]](#)
4. Hage, K.D. Urban-Rural Humidity Differences. *J. Appl. Meteorol.* **1975**, *14*, 1277–1283. [\[CrossRef\]](#)
5. Wang, J.A.; Hutyrá, L.; Li, D.; Friedl, M.A. Gradients of atmospheric temperature and humidity controlled by local urban land-use intensity in Boston. *J. Appl. Meteorol. Climatol.* **2017**, *56*, 817–831. [\[CrossRef\]](#)
6. Hill, A.C.; Mitchell, M.; Yuan, F.; Ruhland, C.T. Intensification of Midwestern Agriculture as a Regional Climate Modifier and Atmospheric Boundary Layer Moisture Source. *Ann. Am. Assoc. Geogr.* **2019**, *109*, 1775–1794. [\[CrossRef\]](#)
7. Theeuwes, N.E.; Barlow, J.; Teuling, A.; Grimmond, C.; Kotthaus, S. Persistent cloud cover over mega-cities linked to surface heat release. *Npj Clim. Atmos. Sci.* **2019**, *2*, 15. [\[CrossRef\]](#)
8. Dou, J.; Wang, Y.; Bornstein, R.; Miao, S. Observed spatial characteristics of Beijing urban climate impacts on summer thunderstorms. *J. Appl. Meteorol. Climatol.* **2015**, *54*, 94–105. [\[CrossRef\]](#)
9. Pielke Sr, R.A.; Adegoke, J.; Beltraán-Przekurat, A.; Hiemstra, C.A.; Lin, J.; Nair, U.S.; Niyogi, D.; Nobis, T.E. An overview of regional land-use and land-cover impacts on rainfall. *Tellus B Chem. Phys. Meteorol.* **2007**, *59*, 587–601. [\[CrossRef\]](#)
10. Shepherd, J.M. A review of current investigations of urban-induced rainfall and recommendations for the future. *Earth Interact.* **2005**, *9*, 1–27. [\[CrossRef\]](#)
11. Ben-Gai, T.; Bitan, A.; Manes, A.; Alpert, P. Long-term change in October rainfall patterns in southern Israel. *Theor. Appl. Climatol.* **1993**, *46*, 209–217. [\[CrossRef\]](#)
12. Dixon, P.G.; Mote, T.L. Patterns and Causes of Atlanta's Urban Heat Island-Initiated Precipitation. *J. Appl. Meteorol.* **2003**, *42*, 1273–1284. [\[CrossRef\]](#)
13. Sailor, D.J. A review of methods for estimating anthropogenic heat and moisture emissions in the urban environment. *Int. J. Climatol.* **2011**, *31*, 189–199. [\[CrossRef\]](#)
14. Daramola, M.T.; Balogun, I.A. Local climate zone classification of surface energy flux distribution within an urban area of a hot-humid tropical city. *Urban Clim.* **2019**, *29*, 100504. [\[CrossRef\]](#)
15. Chen, C.-T.; Roeckner, E.; Soden, B.J. A Comparison of Satellite Observations and Model Simulations of Column-Integrated Moisture and Upper-Tropospheric Humidity. *J. Clim.* **1996**, *9*, 1561–1585. [\[CrossRef\]](#)
16. Uzan, L.; Egert, S.; Khain, P.; Levi, Y.; Vadislavsky, E.; Alpert, P. Ceilometers as planetary boundary layer height detectors and a corrective tool for COSMO and IFS models. *Atmospheric Chem. Phys.* **2020**, *20*, 12177–12192. [\[CrossRef\]](#)
17. Ziv, S.Z.; Alpert, P.; Reuveni, Y. Long-term variability and trends of precipitable water vapour derived from GPS tropospheric path delays over the Eastern Mediterranean. *Int. J. Climatol.* **2021**, *41*, 6433–6454. [\[CrossRef\]](#)
18. Ziv, S.Z.; Yair, Y.; Alpert, P.; Uzan, L.; Reuveni, Y. The diurnal variability of precipitable water vapor derived from GPS tropospheric path delays over the Eastern Mediterranean. *Atmos. Res.* **2021**, *249*, 105307. [\[CrossRef\]](#)
19. Alpert, P.; Rubin, Y. First Daily Mapping of Surface Moisture from Cellular Network Data and Comparison with Both Observations/ECMWF Product. *Geophys. Res. Lett.* **2018**, *45*, 8619–8628. [\[CrossRef\]](#)
20. Messer, H.; Zinevich, A.; Alpert, P. Environmental monitoring by wireless communication networks. *Science* **2006**, *312*, 713. [\[CrossRef\]](#)
21. Leijnse, H.; Uijlenhoet, R.; Stricker, J.N.M. Rainfall measurement using radio links from cellular communication networks. *Water Resour. Res.* **2007**, *43*, 1–6. [\[CrossRef\]](#)
22. Zinevich, A.; Messer, H.; Alpert, P. Frontal rainfall observation by a commercial microwave communication network. *J. Appl. Meteorol. Climatol.* **2009**, *48*, 1317–1334. [\[CrossRef\]](#)
23. Zinevich, A.; Alpert, P.; Messer, H. Estimation of rainfall fields using commercial microwave communication networks of variable density. *Adv. Water Resour.* **2008**, *31*, 1470–1480. [\[CrossRef\]](#)
24. Alpert, P.; Messer, H.; David, N. Meteorology: Mobile networks aid weather monitoring. *Nature* **2016**, *537*, 617. [\[CrossRef\]](#)
25. David, N.; Sendik, Q.; Messer, H.; Alpert, P. Cellular network infrastructure: The future of fog monitoring? *Bull. Am. Meteorol. Soc.* **2015**, *96*, 1687–1698. [\[CrossRef\]](#)
26. David, N.; Alpert, P.; Messer, H. Technical note: Novel method for water vapour monitoring using wireless communication networks measurements. *Atmos. Chem. Phys.* **2009**, *9*, 2413–2418. [\[CrossRef\]](#)
27. David, N. Analyzing the ability to reconstruct the moisture field using commercial microwave network data. *Atmos. Res.* **2019**, *219*, 213–222. [\[CrossRef\]](#)
28. Oharel; David, N.; Alpert, P.; Messer, H. The Potential of Microwave Communication Networks to Detect Dew—Experimental Study. *IEEE J. Sel. Top. Appl. Earth Obs. Remote Sens.* **2015**, *8*, 4396–4404. [\[CrossRef\]](#)
29. David, N.; Gao, H.O. Using Cellular Communication Networks To Detect Air Pollution. *Environ. Sci. Technol.* **2016**, *50*, 9442–9451. [\[CrossRef\]](#)
30. Chwala, C.; Kunstmann, H. Commercial microwave link networks for rainfall observation: Assessment of the current status and future challenges. *WIREs Water* **2019**, *6*. [\[CrossRef\]](#)

31. Ostrometzky, J.; Eshel, A. Empirical Study of the Quantization Induced Bias in Commercial Microwave Links' Min/Max Attenuation Measurements for Rain Monitoring. *Environments* **2018**, *5*, 80. [CrossRef]
32. Ostrometzky, J.; Eshel, A.; Alpert, P.; Messer, H. Induced bias in attenuation measurements taken from commercial microwave links. In Proceedings of the 2017 IEEE International Conference on Acoustics, Speech and Signal Processing (ICASSP), New Orleans, LA, USA, 5–9 March 2017; pp. 3744–3748. [CrossRef]
33. Leijnse, H.; Uijlenhoet, R.; Berne, A. Errors and Uncertainties in Microwave Link Rainfall Estimation Explored Using Drop Size Measurements and High-Resolution Radar Data. *J. Hydrometeorol.* **2010**, *11*, 1330–1344. [CrossRef]
34. Zinevich, A.; Messer, H.; Alpert, P. Prediction of rainfall intensity measurement errors using commercial microwave communication links. *Atmos. Meas. Tech.* **2010**, *3*, 1385–1402. [CrossRef]
35. Eshel, A.; Messer, H.; Kunstmann, H.; Alpert, P.; Chwala, C. Quantitative Analysis of the Performance of Spatial Interpolation Methods for Rainfall Estimation Using Commercial Microwave Links. *J. Hydrometeorol.* **2021**, *22*, 831–843. [CrossRef]
36. Eshel, A.; Ostrometzky, J.; Gat, S.; Alpert, P.; Messer, H. Spatial Reconstruction of Rain Fields From Wireless Telecommunication Networks—Scenario-Dependent Analysis of IDW-Based Algorithms. *IEEE Geosci. Remote Sens. Lett.* **2020**, *17*, 770–774. [CrossRef]
37. Overeem, A.; Leijnse, H.; Uijlenhoet, R. Retrieval algorithm for rainfall mapping from microwave links in a cellular communication network. *Atmos. Meas. Tech.* **2016**, *9*, 2425–2444. [CrossRef]
38. Alpert, P.; Osetinsky, I.; Ziv, B.; Shafir, H. Semi-objective classification for daily synoptic systems: Application to the eastern Mediterranean climate change. *Int. J. Climatol.* **2004**, *24*, 1001–1011. [CrossRef]
39. Goldreich, Y. *The Climate of Israel*; Springer: Boston, MA, USA, 2003. [CrossRef]
40. Skibin, D.; Hod, A. Subjective analysis of mesoscale flow patterns in northern Israel. *J. Appl. Meteorol.* **1979**, *18*, 329–338. [CrossRef]
41. Alpert, P.; Getenio, B.; Zak-Rosenthal, R. One-level modeling for diagnosing surface winds over complex terrain. Part II: Applicability to short-range forecasting. *Mon. Weather. Rev.* **1988**, *116*, 2047–2061. [CrossRef]
42. Liebe, H.J. An updated model for millimeter wave propagation in moist air. *Radio Sci.* **1985**, *20*, 1069–1089. [CrossRef]
43. van Vleck, J.H. The Absorption of Microwaves by Uncondensed Water Vapor. *Phys. Rev.* **1947**, *71*, 425–433. [CrossRef]
44. Yoav, R. A Novel Approach for High Resolution Humidity Mapping Based on Cellular Network Data. *Tel-Aviv*. 2018. Available online: <https://web2.eng.tau.ac.il/wtest/rainlinklab/wp-content/uploads/2020/07/Thesis-Yoav-Rubin.pdf> (accessed on 23 October 2022).
45. Rubin, Y.; Rostkier-Edelstein, D.; Chwala, C.; Alpert, P. Challenges in Diurnal Humidity Analysis from Cellular Microwave Links (CML) over Germany. *Remote Sens.* **2022**, *14*, 2353. [CrossRef]
46. Cressman, G.P. An Operational Objective Analysis System. *Mon. Weather Rev.* **1959**, *87*, 367–374. [CrossRef]
47. Oke, T.R. *Boundary Layer Climates*; Routledge: London, UK; New York, NY, USA, 2002.
48. Landsberg, H.E. *The Urban Climate*; Academic Press: New York, NY, USA.
49. Elhacham, E.; Alpert, P. Impact of coastline-intensive anthropogenic activities on the atmosphere from moderate resolution imaging spectroradiometer (MODIS) data in Dubai (2001–2014). *Earths Future* **2016**, *4*, 54–61. [CrossRef]

Disclaimer/Publisher's Note: The statements, opinions and data contained in all publications are solely those of the individual author(s) and contributor(s) and not of MDPI and/or the editor(s). MDPI and/or the editor(s) disclaim responsibility for any injury to people or property resulting from any ideas, methods, instructions or products referred to in the content.